geotechnics

MDPI

Article

Sensitivity Analysis and Application of the Shanghai Model in Ultra-Deep Excavation Engineering

Aoyang Ma [1,*], Weiyi Wang [1], Wenxuan Zhu [1], Zhonghua Xu [2,3] and Guanlin Ye [1]

[1] Department of Civil Engineering, Shanghai Jiao Tong University, Shanghai 200240, China; wwyvyww@sjtu.edu.cn (W.W.); zhuwx1992@sjtu.edu.cn (W.Z.); ygl@sjtu.edu.cn (G.Y.)
[2] Shanghai Underground Space Engineering Design & Research Institute, East China Architecture Design & Research Institute Co., Ltd., Shanghai 200011, China; xzhzyq@gmail.com
[3] Shanghai Engineering Research Center of Safety Control for Facilities Adjacent to Deep Excavations, Shanghai 200011, China
* Correspondence: ocean-yang@sjtu.edu.cn; Tel.: +86-183-2665-0098

Abstract: In deep foundation pit engineering, the soil undergoes a complex stress path, encompassing both loading and unloading phases. The Shanghai model, an advanced constitutive model, effectively accounts for the soil's deformation characteristics under these varied stress paths, which is essential for accurately predicting the horizontal displacement and surface settlement of the foundation pit's enclosure structure. This model comprises eight material parameters, three initial state parameters, and one small-strain parameter. Despite its sophistication, there is a scarcity of numerical studies exploring the correlation between these parameters and the deformation patterns in foundation pit engineering. This paper initially establishes the superiority of the Shanghai model in ultra-deep circular vertical shaft foundation pit engineering by examining a case study of a nursery circular ultra-deep vertical shaft foundation pit, which is part of the Suzhou River section's deep drainage and storage pipeline system pilot project in Shanghai. Subsequently, utilizing an idealized foundation pit engineering model, a comprehensive sensitivity analysis of the Shanghai model's multi-parameter values across their full range was performed using orthogonal experiments. The findings revealed that the parameter most sensitive to the lateral displacement of the underground continuous wall was κ, with an increase in κ leading to a corresponding increase in displacement. Similarly, the parameter most sensitive to surface subsidence outside the pit was λ, with an increase in λ resulting in greater subsidence. Lastly, the parameter most sensitive to soil uplift at the bottom of the pit was also κ, with an increase in κ leading to more significant uplift.

Keywords: constitutive model; numerical simulation; ultra-deep foundation pit; orthogonal experiment; parameter sensitivity analysis

Academic Editor: Raffaele Di Laora

Received: 29 November 2024
Revised: 27 December 2024
Accepted: 6 January 2025
Published: 13 January 2025

Citation: Ma, A.; Wang, W.; Zhu, W.; Xu, Z.; Ye, G. Sensitivity Analysis and Application of the Shanghai Model in Ultra-Deep Excavation Engineering. *Geotechnics* **2025**, *5*, 6. https://doi.org/10.3390/geotechnics5010006

1. Introduction

As computer technology, numerical analysis methods, and soil constitutive relationships advance, numerical analysis has emerged as the most effective tool for analyzing deep excavation engineering. A critical aspect of numerical analysis is the selection of appropriate constitutive models and calculation parameters [1,2].

For instance, in the numerical analysis of foundation pit engineering in soft soil regions with sensitive surroundings, the Small-Strain Hardening Model (HSS model) is prevalent in the engineering community. However, the Shanghai model, as referenced in various studies (Zhang et al. [3]; Taiebat and Dafalias [4]; Yin et al. [5]; Zhou and Sheng [6]), offers

a comprehensive description of the diverse characteristics of soft soil. It accounts for different soil types, small-strain behavior, alternating motion, liquefaction, shear dilation or shrinkage, and other factors, thereby meeting the demands of various geotechnical engineering projects.

The Shanghai model is continuously evolving, with parameters being added to the structural development function of existing constitutive models. This innovation characterizes the distinct effects of plastic shear strain and plastic volume strain on soil structure, enabling the model to more accurately reflect the structural development characteristics of different soil layers in Shanghai. By leveraging the relationship between the stress ratio and the shear dilation ratio in true triaxial tests on normally consolidated remolded clay, a modified plastic potential equation has been developed in the transformed stress space. This development accounts for the influence of stress paths on soil strength and volume deformation, broadening the applicability of the constitutive equation to complex stress states encountered in engineering practice. Furthermore, the model's shear modulus for natural clay in the small-strain range has been enhanced by integrating classical small-strain stiffness theory. This allows the constitutive model to capture the initial high modulus and nonlinear attenuation characteristics of natural clay under small-strain conditions, aligning with the actual deformation observed in soft soil engineering [7–10].

The Shanghai model's superiority in addressing engineering problems in soft soil areas has spurred numerous studies on parameter selection methods, further enhancing its application. Sheng Jiaren et al. [11] systematically investigated the physical and mechanical properties of clay layers in Shanghai, establishing for the first time an exponential relationship between the compression index and natural moisture content of Shanghai clay, as well as the impact of structural factors on soil compressibility, shear strength, bulk deformation, and excess pore pressure. Yang Tongshuai et al. [12] studied the small-strain characteristics of Shanghai clay, demonstrating that empirical formulas considering the soil stress state, porosity ratio, and overconsolidation ratio can accurately describe the initial shear modulus of soft soil layers in Shanghai. Lin Tianxiang et al. [13] conducted research on shallow soil layers in Shanghai, refining the method for determining the parameters of the Shanghai soil constitutive model.

Despite the Shanghai model's advantages, simple models such as the M-C model and HSS model are still widely employed in current numerical analyses of urban deep excavation engineering [14,15]. There is a need to improve the consistency between simulated and measured values and to clarify the impact of advanced constitutive parameters, such as those in the Shanghai model, on calculation outcomes [16,17].

This article evaluates the suitability of the Shanghai model for circular ultra-deep foundation pit engineering, using the Miaopu shaft circular excavation of the deep tunnel sewerage project of Suzhou River in Shanghai [18,19]. Concurrently, to build a repository of experience regarding the parameter values of the Shanghai model in foundation pit engineering, a comprehensive sensitivity analysis across multiple parameters was conducted. This analysis was based on orthogonal experiments applied to an idealized foundation pit engineering scenario. This study aims to elucidate the effects of parameter value variations on computational outcomes and to pinpoint high-sensitivity parameters that are crucial for accurate modeling. The specific research method is shown in Figure 1.

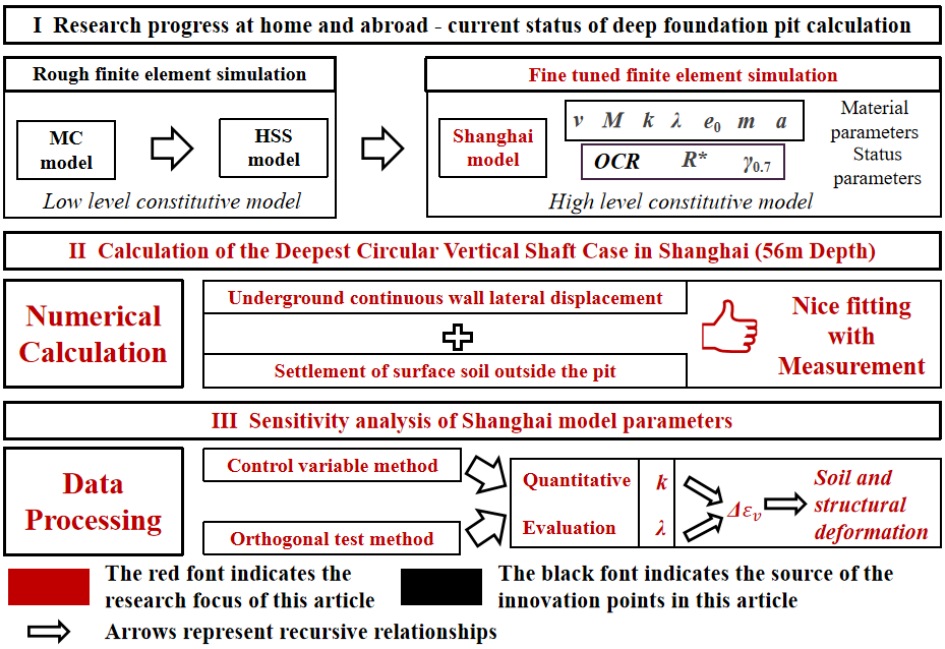

Figure 1. Numerical research path of deep excavation engineering based on Shanghai model.

2. Introduction to Shanghai Model

2.1. Principles of Shanghai Model Mechanics

The anisotropy of soil and its control parameters are not considered in this article [20–22]. Figure 2 shows the current stress state, overconsolidation state, and structural state of soil, as well as the corresponding subloading surface, normal loading surface, and superloading surface. The point A (p,q) in the figure represents the current stress state of the soil, and the surface passing through this point is the lower load surface; point B (p^*,q^*) represents the normal consolidation stress state of the remolded soil, and the surface passing through this point is the normal consolidation yield surface; and point C $(\overline{p},\overline{q})$ represents the normal consolidation stress state of natural soil, and the surface passing through this point is the superloading surface. The three vertical dashed lines in Figure 2 represent the failure strength of the yield surface of three different soil states.

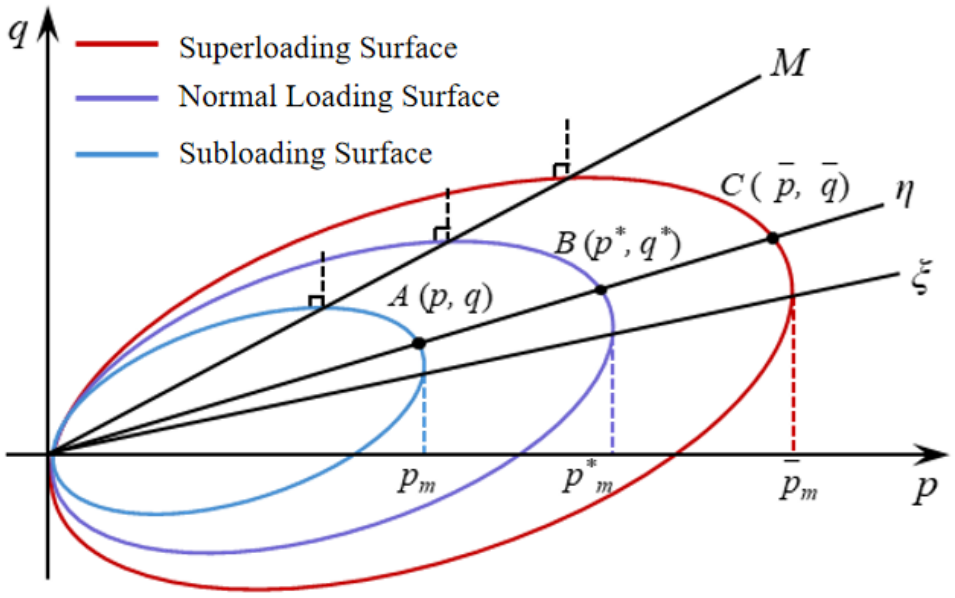

Figure 2. Superloading surface, normal yield surface, and subloading surface of soil.

The three yield surfaces through points *A*, *B*, and *C* are geometrically similar. The ratio of the normal yield surface to the superloading surface is defined as *R**, and the ratio of the subloading surface to the superloading surface is defined as *R*, where the reciprocal of the initial *R* is defined as the overconsolidation ratio, denoted as *OCR* (*OCR* ≥ 1). Then, there are the following relationships:

$$R^* = \frac{p^*}{\overline{p}} = \frac{q^*}{\overline{q}}, 0 < R^* \leq 1, \frac{q^*}{p^*} = \frac{\overline{q}}{\overline{p}} \tag{1}$$

$$R = \frac{p}{\overline{p}} = \frac{q}{\overline{q}}, 0 < R \leq 1, \frac{q}{p} = \frac{\overline{q}}{\overline{p}} \tag{2}$$

For the current stress state of soil on the subloading surface, its yield surface can be expressed as follows:

$$f = \ln \frac{\widetilde{p}}{\widetilde{p}_0} + \ln \frac{M^2 - \zeta^2 + \eta^{*2}}{M^2 - \zeta^2} + \ln R^* - \ln R - \frac{\varepsilon_v^p}{C_p} \tag{3}$$

In Equation (3), $\widetilde{p}$ is the average effective stress; $\widetilde{p}_0 = 98$kPa is the reference stress; ε_v^p is the strain of a plastic body; β_{ij} is the anisotropic stress tensor; $\eta^* = \widetilde{\eta}^* = \sqrt{\frac{3}{2}\hat{\eta}_{ij}\hat{\eta}_{ij}}$, where $\hat{\eta}_{ij} = \eta_{ij} - \beta_{ij}$ is the difference between the stress ratio tensor, η_{ij}, and the anisotropic stress tensor, β_{ij}; and $C_p = \frac{\lambda - \kappa}{1 + e_0}$, where λ and κ represent the compression index and rebound index of the soil, respectively, and e_0 is the reference porosity ratio under reference stress $\widetilde{p}_0 = 98$ kPa.

The model adopts the associated flow rule, as shown in Equation (4):

$$d\varepsilon_{ij}^p = \Lambda \frac{\partial f}{\partial \sigma_{ij}} \tag{4}$$

In Equation (4), Λ is the plasticity factor, which can be determined based on the coordination equation of the subloading surface. The coordination equation for the subloading surface is shown in Equation (5).

$$df = 0 \rightarrow \frac{\partial f}{\partial \sigma_{ij}} d\sigma_{ij} + \frac{\partial f}{\partial \beta_{ij}} d\beta_{ij} + \frac{1}{R^*} dR^* - \frac{1}{R} dR - \frac{1}{C_p} d\varepsilon_v^p = 0 \tag{5}$$

In addition, the unified constitutive model also provides development equations for structural state parameters, overconsolidation state parameters, and anisotropic state parameters, which are introduced as follows.

2.1.1. Structural State Parameter Development Equation

$$dR^* = U^* d\varepsilon_d^p \tag{6}$$

$$U^* = \frac{aM}{C_p} R^* (1 - R^*) (0 < R^* \leq 1) \tag{7}$$

In Equations (6) and (7), material parameter *a* is a structural control parameter, and its value reflects the rate of the structural failure of the soil during the shear process. $d\varepsilon_d^p$ is the incremental plastic strain.

2.1.2. Development Equation of Overconsolidation State Parameters

In the constitutive model, it is believed that the change in the overconsolidation degree of soil during the shear process is related to two factors, namely the change in plastic strain

and the development of anisotropy. The development equation of overconsolidation is as follows:

$$dR = U\left\|d\varepsilon_{ij}^{p}\right\| + R\frac{\eta}{M}\frac{\partial f}{\partial \beta_{ij}}d\beta_{ij} \tag{8}$$

In Equation (8), $\left\|d\varepsilon_{ij}^{p}\right\|$ and U are, respectively, represented as follows:

$$\left\|d\varepsilon_{ij}^{p}\right\| = \sqrt{d\varepsilon_{ij}^{p}d\varepsilon_{ij}^{p}} = \Lambda\sqrt{\frac{\partial f}{\partial \sigma_{ij}}\frac{\partial f}{\partial \sigma_{ij}}} = \Lambda\frac{\sqrt{6\eta^{*2} + \frac{1}{3}\left(M^2 - \eta^2\right)^2}}{\left(M^2 - \xi^2 + \eta^{*2}\right)\widetilde{p}} \tag{9}$$

$$U = -\frac{mM}{C_p}\left[\frac{\left(\widetilde{p}/\widetilde{p}_0\right)^2}{\left(\widetilde{p}/\widetilde{p}_0\right)^2 + 1}\right]\ln R \tag{10}$$

In Equations (9) and (10), $\widetilde{p}_0 = 98\text{kPa}$ is the reference stress. Using atmospheric pressure as a reference stress can simplify the analysis of soil stress state. Due to the fact that, in most cases, the pore water pressure in soil can be approximated as atmospheric pressure, the material parameter m is a control parameter for overconsolidation, and its value reflects the rate of overconsolidation dissipation of the soil during the shear process (the larger the value, the faster the overconsolidation dissipation of the soil).

2.1.3. Development Equation of Anisotropic State Parameters

$$d\beta_{ij} = \frac{M}{C_p}b_r(M - \xi)d\varepsilon_d^p\frac{\hat{\eta}_{ij}}{\left\|\hat{\eta}_{ij}\right\|} = \sqrt{\frac{3}{2}}\frac{M}{C_p}b_r(M - \xi)d\varepsilon_d^p\frac{\hat{\eta}_{ij}}{\eta^*} \tag{11}$$

In Equation (11), the material parameter b_r is an anisotropic control parameter used to control the rate of soil anisotropy development during shear or compression.

The increment of the strain tensor includes two parts: the elastic and plastic parts,$d\varepsilon_{kl} = d\varepsilon_{kl}^{e} + d\varepsilon_{kl}^{p}$. Therefore, the increment of the stress tensor, $d\sigma_{ij}$, can be expressed as follows:

$$\begin{aligned} d\sigma_{ij} &= E_{ijkl}d\varepsilon_{kl}^{e} = E_{ijkl}\left(d\varepsilon_{kl} - d\varepsilon_{kl}^{p}\right) \\ &= E_{ijkl}d\varepsilon_{kl} - \Lambda E_{ijkl}\frac{\partial f}{\partial \sigma_{kl}} \end{aligned} \tag{12}$$

In Equation (12), $d\sigma_{ij}$ is the stress increment tensor; $d\varepsilon_{kl}^{p}$ is the plastic strain increment tensor; and E_{ijkl} is an elastic constitutive tensor, expressed as follows:

$$E_{ijkl} = \lambda_{Lame}\delta_{ij}\delta_{kl} + G\left(\delta_{ik}\delta_{jl} + \delta_{il}\delta_{jk}\right) \tag{13}$$

In Equation (13), λ is the Lame constant and G is the shear modulus.

By substituting Equations (6–8), (11), and (12) into Equation (5), the plasticity factor, Λ, can be expressed as follows:

$$\Lambda = \frac{\frac{\partial f}{\partial \sigma_{ij}}E_{ijkl}d\varepsilon_{kl}}{h_p + \frac{\partial f}{\partial \sigma_{ij}}E_{ijkl}\frac{\partial f}{\partial \sigma_{kl}}} \tag{14}$$

In Equation (14), the definition of variable h_p is as follows:

$$h_p = \frac{1}{C_p\left(M^2 - \zeta^2 + \eta^{*2}\right)\sigma_m}\left[M_\mathrm{s}^2 - \eta^2\right] \tag{15}$$

In Equation (15), the definition of variable M_s is as follows:

$$M_s^2 = M^2 - \frac{mM\ln R}{R}\left[\frac{(\tilde{p}/\tilde{p}_0)^2}{(\tilde{p}/\tilde{p}_0)^2+1}\right]\sqrt{6\eta^{*2}+\frac{1}{3}(M^2-\eta^2)^2} \\ -2aM(1-R^*)\eta^* + (1-\frac{\eta}{M})\frac{\sqrt{6}Mb_r(M-\zeta)\eta^{*2}(2M^2-3\eta_{ij}\beta_{ij})}{(M^2-\zeta^2+\eta^{*2})(M^2-\zeta^2)} \tag{16}$$

The loading criteria for the model are the same as those suggested by Asaoka et al. (1994 [23]; 2002 [24]), as follows:

$$\begin{cases} \Lambda > 0 & \text{Loading} \\ \Lambda = 0 & \text{Neutral loading} \\ \Lambda < 0 & \text{Unloading} \end{cases} \tag{17}$$

2.1.4. Soil Small-Strain Stiffness Correction

Based on extensive engineering practice, Burland (1989 [25]) summarized and found that soil strain mainly ranges from 0.01% to 1% and revised the Shanghai model accordingly.

Considering the attenuation of soil shear stiffness, the shear modulus attenuation equation (Santos and Correia, 2001 [26]) is adopted as follows:

$$G = \begin{cases} \left.\frac{G_0}{(1+a\gamma/\gamma_{0.7})^2}\right|_{a=3/7} & \gamma < \gamma_c \\ \frac{E}{2(1+\nu)} & \gamma \geq \gamma_c \end{cases} \tag{18}$$

In Equation (18), G_0 is the initial shear modulus and γ_c is the shear strain threshold for small strains. When the shear modulus decreases to 70% of its initial value, the corresponding shear strain is $\gamma_{0.7}$. By substituting Equation (18) into Equation (13), a description of small-strain mechanical properties can be achieved in the original constitutive model.

In order to minimize the number of parameters as much as possible while accurately describing the properties, considering the continuity of the shear modulus attenuation curve, a shear strain threshold can be assumed to inversely solve for the initial shear modulus, G_0, as shown below.

$$\frac{G_0}{(1+a\gamma/\gamma_{0.7})^2} = \frac{E}{2(1+\nu)} \rightarrow G_0 = \frac{(1+0.001a/\gamma_{0.7})^2}{2(1+\nu)}E \tag{19}$$

By substituting Equation (19) into Equation (18), the initial shear modulus, G_0, can be replaced, and Equation (18) can be rewritten as follows:

$$G = \begin{cases} \left.\left(\frac{1+0.001a/\gamma_{0.7}}{1+\gamma a/\gamma_{0.7}}\right)^2\frac{E}{2(1+\nu)}\right|_{a=3/7} & \gamma < \gamma_c \\ \frac{E}{2(1+\nu)} & \gamma \geq \gamma_c \end{cases} \tag{20}$$

In Equation (20), E is the elastic modulus, which is expressed as follows:

$$E = \frac{3(1-2\nu)(1+e_0)}{\kappa}\widetilde{p}_0 \tag{21}$$

In Equation (21), $\widetilde{p}_0$ is the reference stress. Due to the fact that, in most cases, the pore water pressure in soil can be approximated as atmospheric pressure, using atmospheric pressure as a reference stress can simplify the analysis of soil stress state. E_0 is the porosity ratio under the reference stress; and κ and v represent the rebound index and Poisson's ratio of the soil [10].

2.2. Introduction to Shanghai Model Parameters

The Shanghai model is an advanced elastoplastic model with 12 parameters, including 8 material parameters, 3 initial state parameters, and 1 small-strain parameter, as shown in Figure 3.

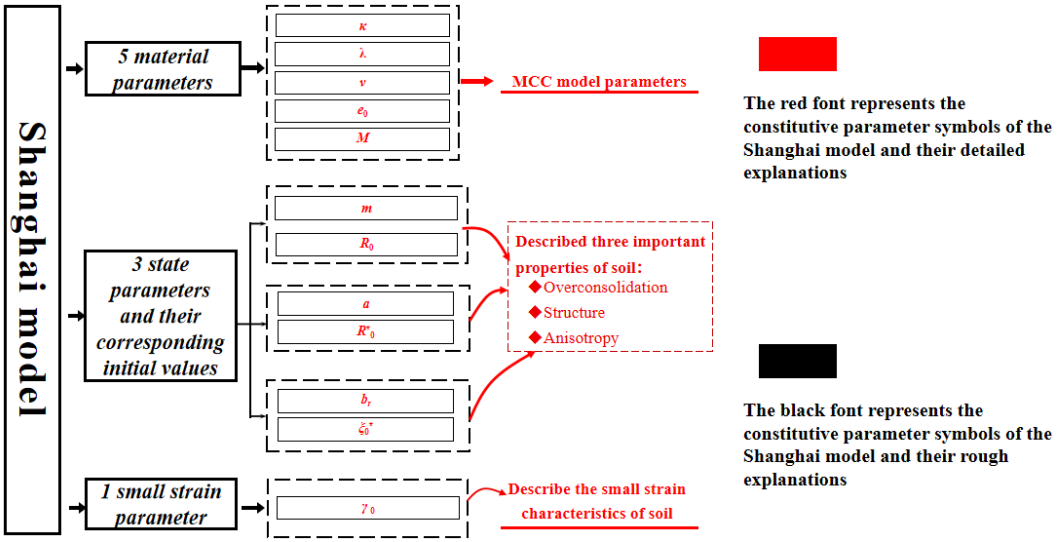

Figure 3. Introduction to constitutive parameters of Shanghai model.

The eight material parameters of the constitutive model are the reference porosity e_0, the Poisson's ratio v, the slope of the critical state line M, the compression index λ, the rebound index κ, the over consolidation control parameter m, the structural control parameter a, and the anisotropy control parameter b_r. The material parameters include five modified Cambridge model parameters. The three initial state parameters are the initial overconsolidation degree R_0 ($R_0 = 1/OCR$), the initial structural parameter R^*_0, and the initial anisotropy parameter. These three initial state parameters (R_0, R^*_0, and the initial anisotropy parameter) correspond to three material control parameters (m, a, and b_r), which are used to describe the overconsolidation, structural, and anisotropic properties of the soil, respectively. The small-strain parameter $\gamma_{0.7}$ represents the shear strain corresponding to a decrease in the shear modulus to 70% of its initial value.

In the Shanghai model, stress-induced anisotropy is mainly reflected in cyclic loading, while the stress-induced anisotropy generated during the shearing process in foundation pit engineering is relatively small, and its influence on the stress–strain relationship can be ignored (Yu Yalei et al., 2016 [27]).

3. Engineering Verification of Parameter Selection Scheme for Shanghai Model

3.1. Engineering Background

The pilot project for the deep drainage and storage pipeline system of the Suzhou River section in Shanghai is the Miaopu Yunling West section storage system. The Miaopu section storage system is located at the junction of Fuquan North Road and Linhong Road in Changning District, Shanghai. The Miaopu section includes vertical shafts (Zone I) and surrounding comprehensive facilities (Zones II-V). The planar distribution and measurement point layout of each zone are shown in Figure 4. Among them, the vertical shaft is arranged in a circular shape, with an inner diameter of 30 m and a base burial depth of 56.3 m.

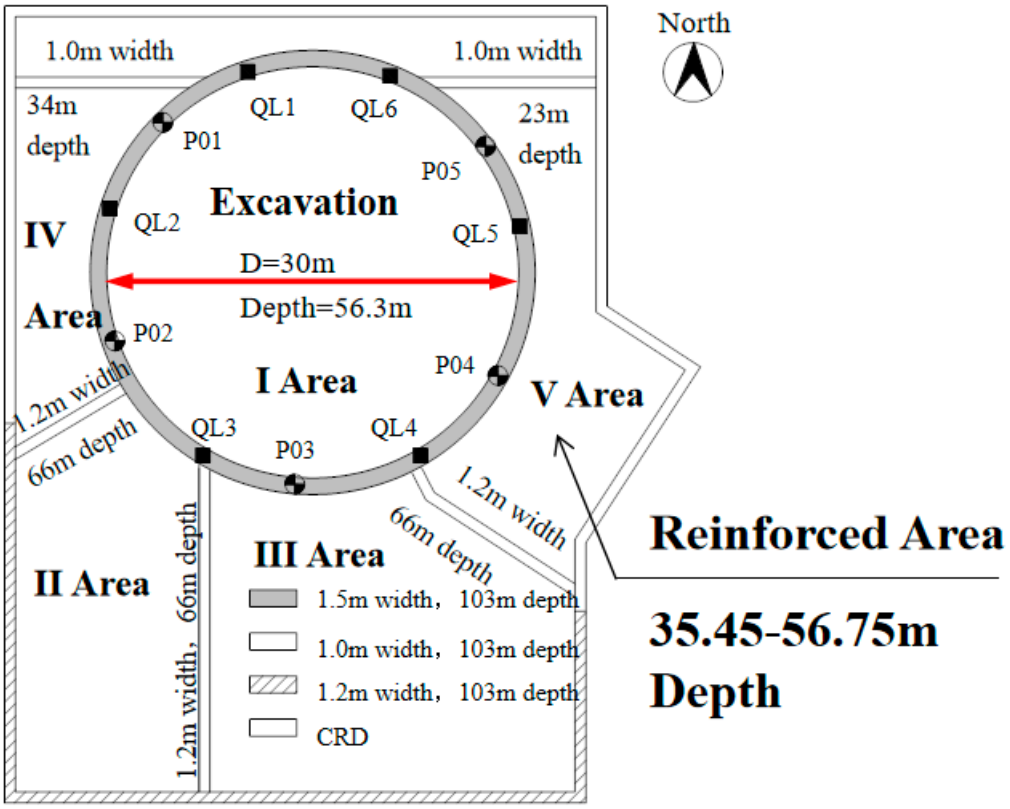

Figure 4. Layout of measurement points and structural parameters for deep foundation pit engineering in Miaopu.

3.2. Finite Element Model

The optimized support scheme was analyzed using Plaxis3D software (2022) to establish a three-dimensional finite element model of the foundation pit considering the combined action of the soil and structure [28]. The calculation model includes the soil, the underground continuous wall system around the foundation pit, and the ring beam system. The three-dimensional finite element calculation model of the foundation pit is shown in Figure 5. The soil is simulated using 10-node wedge-shaped solid elements, the underground continuous wall system of the foundation pit is simulated using 6-node triangular plate shell elements, and the temporary ring beam is simulated using 3-node beam elements. The entire model is divided into 689,127 units and 990,328 nodes. The determination of the soil's geometric dimensions is based on the specified deformation limits of the soil surrounding the excavation, as outlined in the excavation engineering specifications.

The horizontal boundary distance of the foundation pit is taken as 6 times the excavation depth of the foundation pit, and the soil depth is about 3 times the excavation depth, which is sufficient to cover the deformation impact range of the surrounding soil of the foundation pit. The side of the model constrains the horizontal displacement, while the bottom constrains both the horizontal and vertical displacement. The seepage boundary conditions are that the side adopts a constant head seepage boundary and the bottom is an impermeable boundary. The seepage boundary water head of the first to fifth layers of soil is set to an average water head of 0.5 m at the groundwater level, the seventh layer is the first confined aquifer with a depth of 4 m at the confined water level, the ninth layer is the second confined aquifer with a depth of 5 m at the confined water level, and the tenth layers A and I1 are the third confined aquifer with a depth of 5.5 m at the confined water level [19].

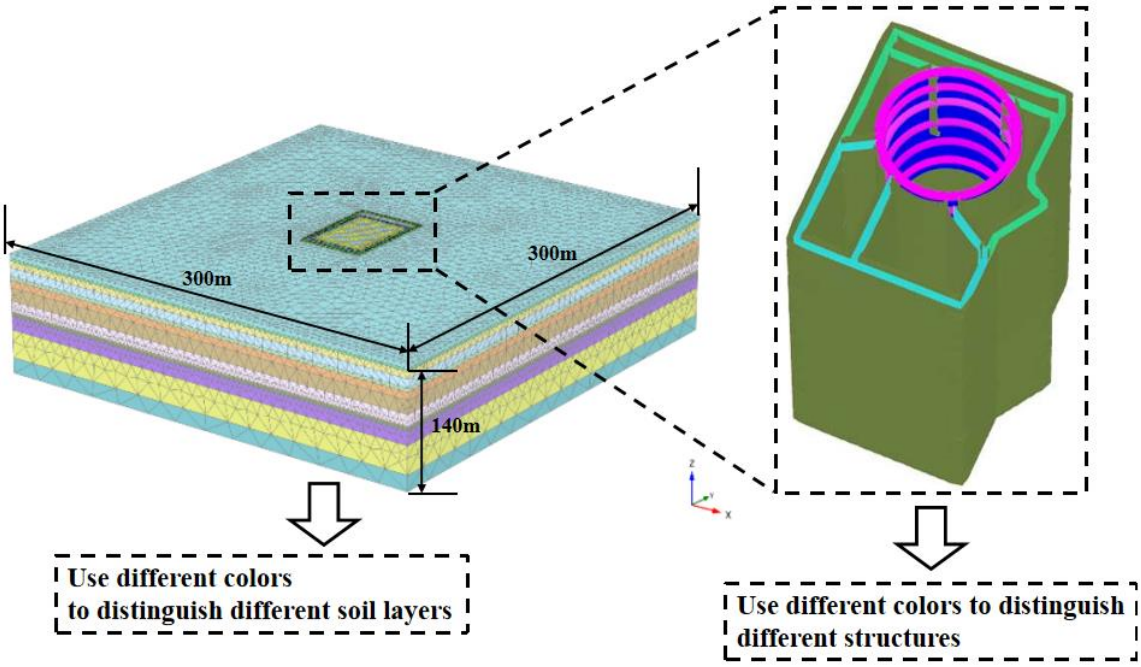

Figure 5. Three-dimensional finite element calculation model of Miaopu foundation pit.

3.3. Calculation Parameters of Constitutive Model

The accuracy of the simulation values for soil and structural deformation in deep foundation pit engineering is high. The Shanghai model, as an advanced constitutive model that can accurately describe the deformation of soft clay and sandy soil, has strong applicability value for Miaopu deep foundation pit engineering in this case. Therefore, in order to accurately analyze the deformation of the soil and structure of the Miaopu foundation pit, the Shanghai model was used to complete its finite element numerical simulation analysis.

Based on the Shanghai model theory introduced in the first section and the geological survey data of Miaopu engineering, the calculation parameters of the Shanghai model are determined as shown in Table 1.

Table 1. Excavation stage of ultra-deep circular vertical shaft excavation construction in Miaopu.

Construction Conditions	Construction Content	Construction Time
Excavation 1	Excavate the foundation pit to an elevation of −2.5 m	30 d
Excavation 2	Excavate the foundation pit to an elevation of −10 m, forming the first support	30 d
Excavation 3	Excavate the foundation pit to an elevation of −18.45 m to form a second support	30 d
Excavation 4	Excavate the foundation pit to an elevation of −29.55 m, forming a third support	30 d
Excavation 5	Excavate the foundation pit to an elevation of −40 m, forming a fourth support	30 d
Excavation 6	Excavate the foundation pit to an elevation of −50 m, forming a fifth support	30 d
Excavation 7	Excavate the foundation pit to an elevation of −56.3 m, forming a sixth support	30 d

3.4. Underground Continuous Wall Lateral Displacement

From Figure 6, it can be seen that the location with the maximum lateral deformation of the wall [29] mainly occurs near the elevation of the excavation face, corresponding to the

maximum values of the X-directional displacement and Y-directional displacement of the underground continuous wall of the circular vertical shaft in Miaopu, which are 12.0 and 13.3 mm, respectively. The total deformation of the vertical shaft wall is relatively uniform, and under the influence of the circumferential spatial effect, the overall deformation of the wall is relatively small, only 0.03% of the excavation depth, fully meeting the deformation control requirements.

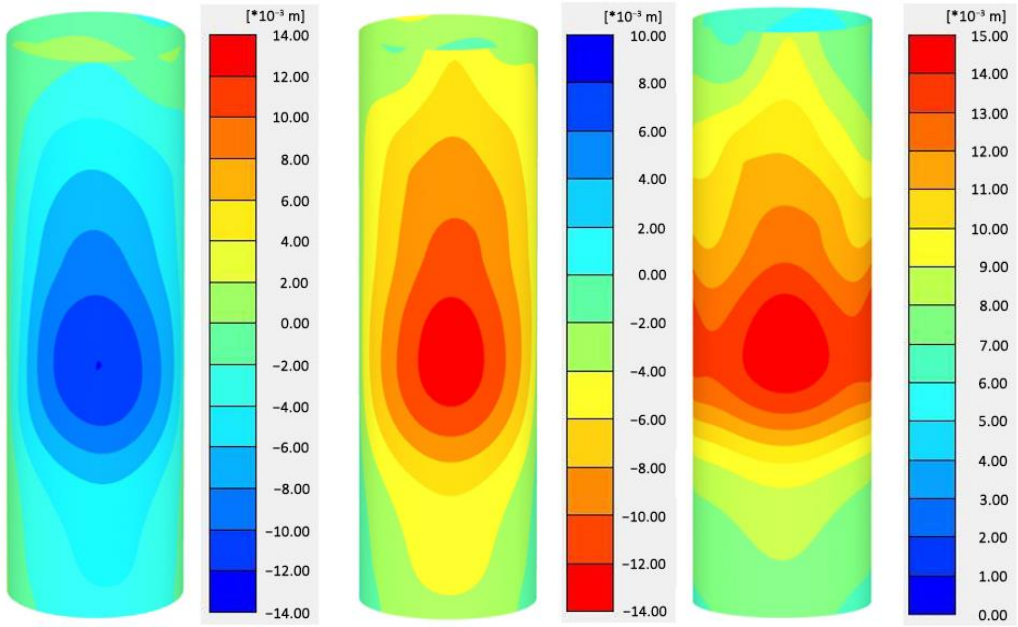

Figure 6. Finite element results of lateral displacement of underground continuous wall upon completion of foundation pit construction. (**a**) X-directional displacement of underground continuous wall (east side); (**b**) Y-direction displacement of underground continuous wall (north side); (**c**) total displacement of underground continuous wall.

As the deepest circular soft soil foundation pit in Shanghai, the Miaopu pit has great research value. Figure 7 shows a comparison between the constitutive simulation results of measuring points P01, P02, and P05 and the on-site measured results. It can be seen from Figure 7 that the lateral displacement of the underground continuous wall calculated by the Shanghai model is basically consistent with the measured deformation law. The deformation of each measuring point gradually increases with the increase in excavation depth, and the position where the maximum deformation occurs gradually moves downwards. The overall deformation shape is "spindle-shaped".

3.5. Settlement of Surface Soil Outside the Foundation Pit

The vertical deformation cloud map of the foundation pit and surrounding soil [30,31] obtained from the finite element analysis is shown in Figure 8. From the figure, it can be observed that due to the limitation of the underground continuous wall of the comprehensive facility around the vertical shaft, the surface settlement outside the pit mainly occurs between the vertical shaft and the underground continuous wall of the comprehensive facility, with a maximum settlement value of 8 mm. The settlement value outside the comprehensive facilities is relatively small, with a maximum settlement value of only about 4 mm, which meets the requirements for surface settlement control.

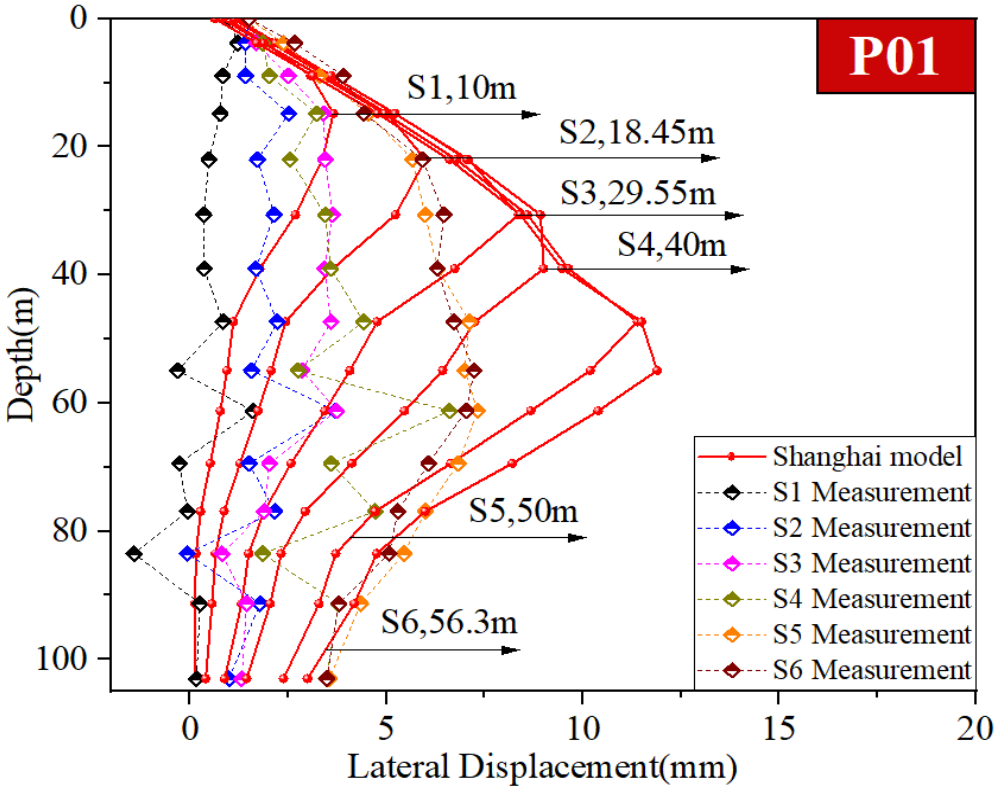

(**a**) P01 measurement point.

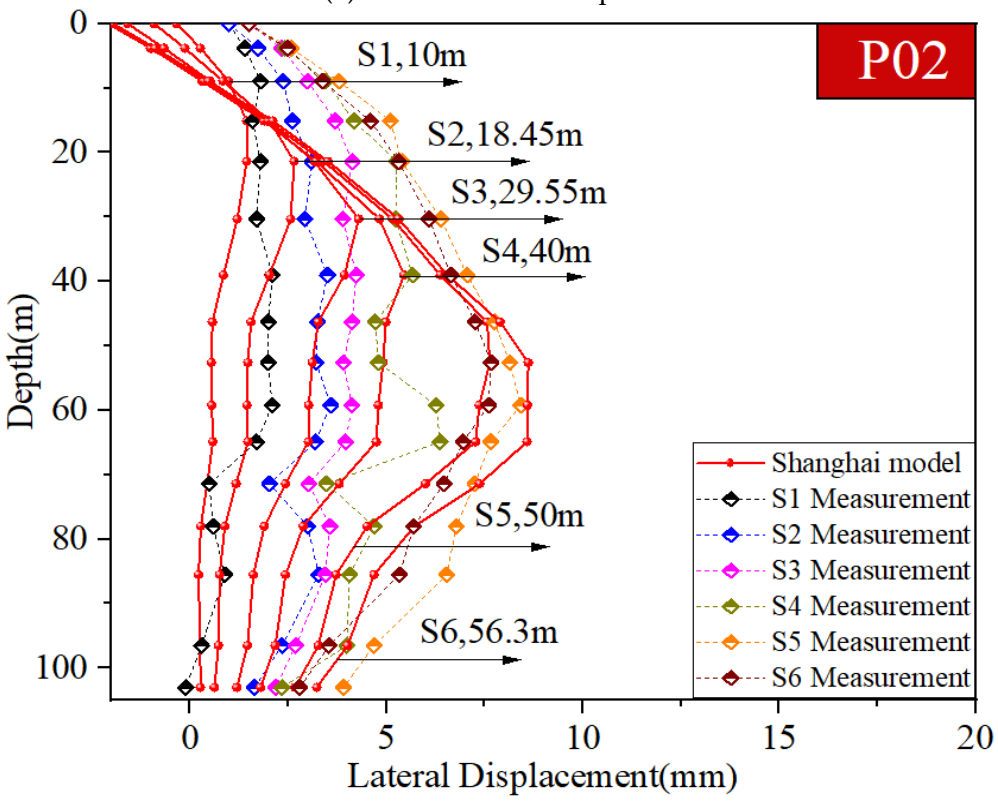

(**b**) P02 measurement point

Figure 7. *Cont*.

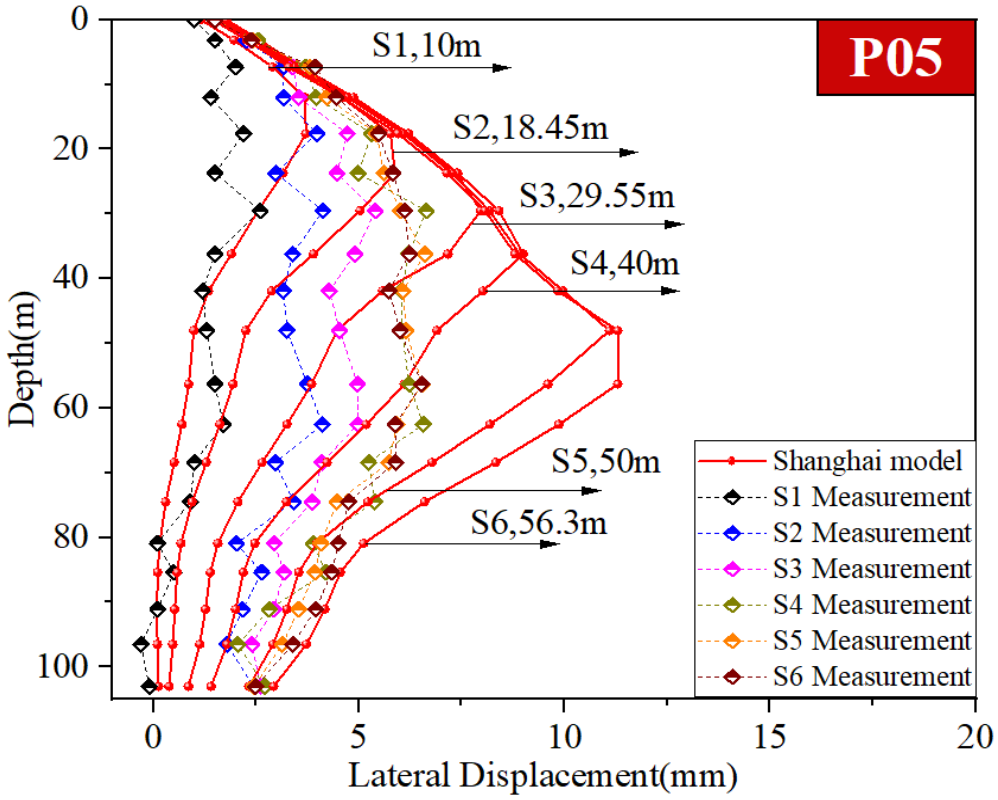

(**c**) P05 measurement point

Figure 7. Comparison between the calculation results and actual measurements of the lateral displacement of the underground continuous wall at each stage.

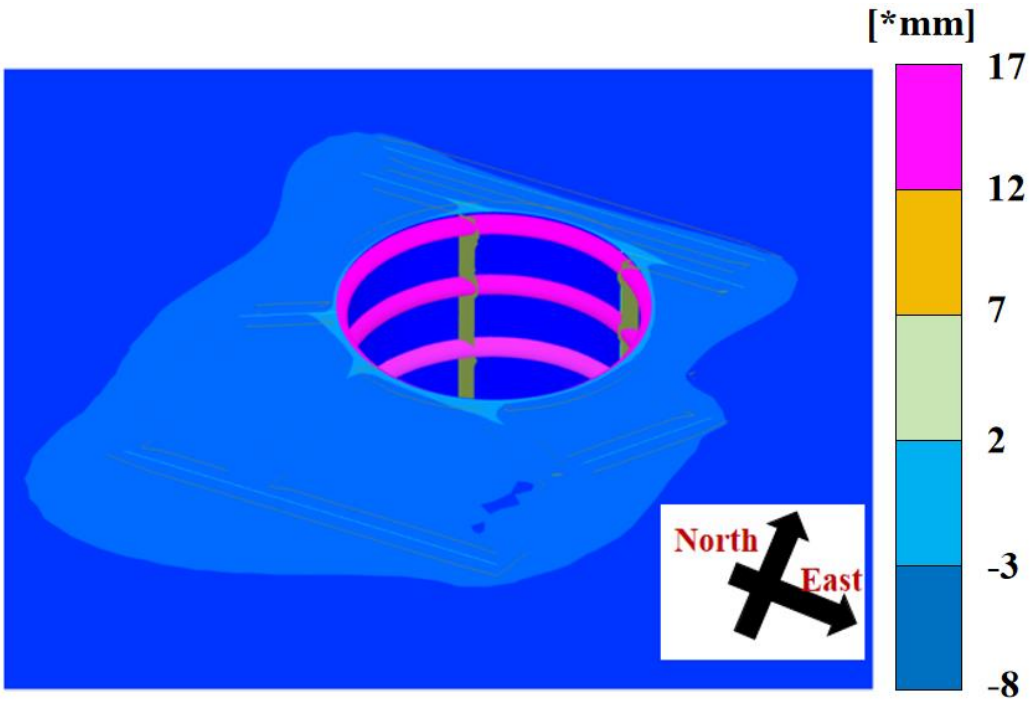

Figure 8. Finite element results of surface settlement outside the pit.

Taking the surface settlement on the east side as an example and comparing the simulation results with the on-site measurement results, it was found that the calculated and measured surface settlement shapes were both groove-shaped, which is basically consistent with the surface settlement law of medium- and shallow-depth foundation pits in soft soil strata. The computational outcomes of the Shanghai model have effectively mirrored the empirical measurement data. The specific results are shown in Figure 9.

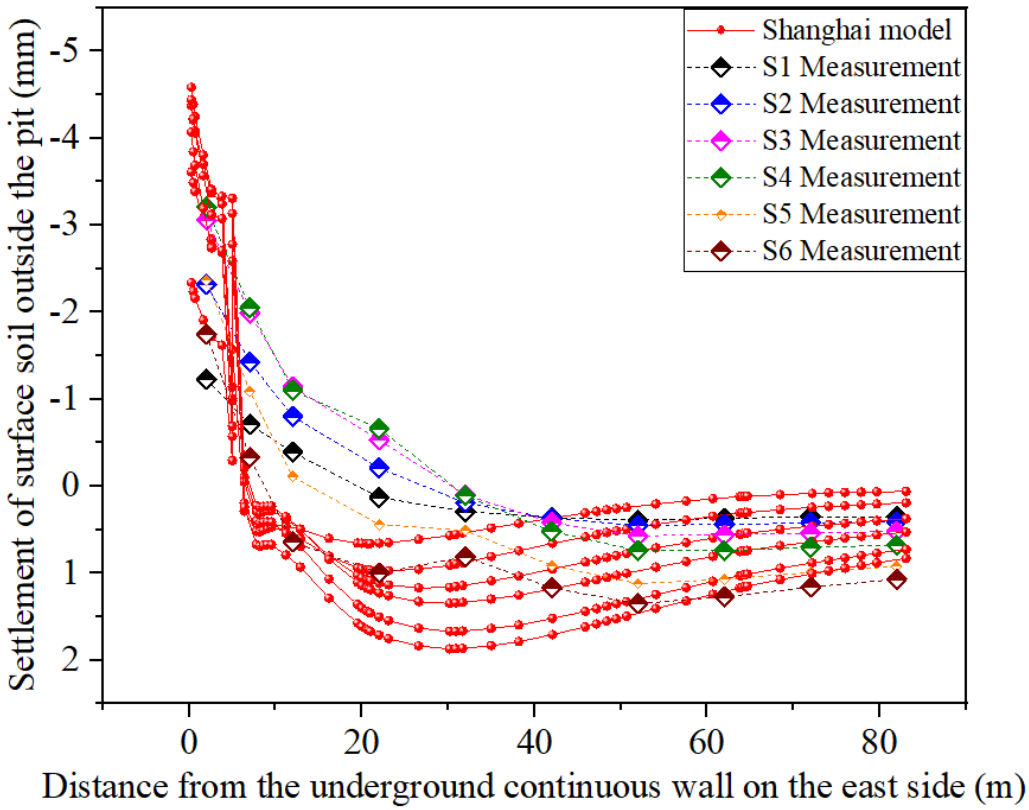

Figure 9. Comparison between the calculated and measured settlement results of the surface soil outside the pit.

4. Sensitivity Analysis of Shanghai Model Parameters for Ideal Foundation Pit Engineering

4.1. Ideal Foundation Pit Engineering Model

A simple ideal foundation pit engineering model was constructed for the parameter sensitivity analysis [32,33]. This model simplifies the formation into a single soil layer, without considering the effect of groundwater. In terms of geometric parameters, the excavation depth of the foundation pit is 20 m, the depth of the retaining structure of the diaphragm wall is 40 m, and the groundwater is located 0.5 m below the surface. The excavation of the foundation pit was carried out in four steps, and three horizontal supports were installed. In terms of the material parameters, the compressive stiffness of the retaining structure of the diaphragm wall was set to 7.5×10^6 kN/m, and its bending stiffness was 1.0×10^6 kN/m. The horizontal support stiffness was set to 2.0×10^6 kN/m, as shown in Figure 10.

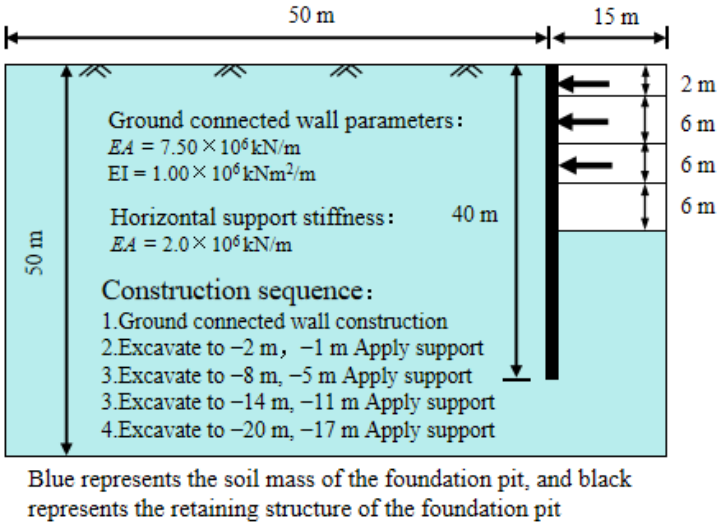

Figure 10. Sensitivity study model of excavation engineering parameters.

4.2. Parameter Values for Shanghai Model

Due to the minimal stress-induced anisotropy generated by the surrounding soil during the excavation of the foundation pit, the influence on the stress–strain relationship can be ignored. In addition, the slope, M, of the critical state line and the initial porosity, e_0, were obtained from laboratory tests and triaxial shear tests on normally consolidated remolded soil. The Poisson's ratio, v, was selected based on experience, so the final parameter value scheme for the Shanghai model is shown in Table 2.

Table 2. Shanghai model parameters for each soil layer in Miaopu.

Layer	e_0	λ	κ	λ Strengthened	κ Strengthened	v	M	OCR	R^*	m	m^*
1	0.756	0.052	0.0104	0.017	0.0035	0.32	1.07	5.5	1	0.7	1
2	1.08	0.072	0.0143	0.024	0.0048	0.33	0.87	1	0.8	4	0.4
3	0.86	0.117	0.0234	0.039	0.0078	0.34	0.77	1.2	0.2	5	0.1
4	0.815	0.109	0.0217	0.036	0.0072	0.34	0.90	1.3	0.6	1.5	0.1
5	0.8	0.063	0.0126	0.021	0.0042	0.29	1.10	2	0.8	1.5	0.1
6	0.81	0.061	0.0122	0.020	0.0041	0.32	1.01	1.2	0.8	0.7	1
7	0.81	0.039	0.0078	0.013	0.0026	0.26	1.10	2	0.8	1.5	0.1
8	0.762	0.020	0.0039	0.007	0.0013	0.24	1.2	10	0.8	0.02	1.5
9	0.81	0.067	0.0135	0.022	0.0045	0.30	0.98	2	0.8	0.5	1
10	0.762	0.020	0.0039	0.007	0.0013	0.23	1.2	10	0.8	0.02	1.5
11	0.762	0.020	0.0039	0.007	0.0013	0.23	1.2	10	0.8	0.02	1.5

However, considering the actual numerical foundation pit engineering calculation required to fit the measured values on site, the complete parameters of the constitutive model are usually determined by back analysis. Starting from the Shanghai model, the key parameters that directly affect soil deformation during excavation are λ and κ.

$$d\varepsilon_v = \frac{1}{v}\left[(\lambda-\kappa)\frac{2\eta d\eta}{M^2+\eta^2} + \lambda\frac{dp'}{p'}\right] \tag{22}$$

$$d\varepsilon_s = \frac{\lambda-\kappa}{v}\left(\frac{2\eta}{M^2+\eta^2}\right)\left(\frac{2\eta}{M^2+\eta^2} + \frac{dp'}{p'}\right) \tag{23}$$

In the formula, $d\varepsilon_v$ and $d\varepsilon_s$ represent the increment of volumetric strain and shear strain, respectively; v is Poisson's ratio; λ is the slope of the normal consolidation line; κ is the slope of the unloading rebound line; and η is the effective stress ratio.

Therefore, two parameters, λ and κ, were selected as sensitivity research objects to investigate the impact of changes in each research parameter on the model calculation results. Combining the range of values and mutual constraints of each parameter, six levels of values were taken for the two research parameters [34,35], as shown in Table 3.

Table 3. Evaluation of partial parameters of Shanghai model.

Parameter	Empirical Formulas and Accuracy	Value
e_0 (p = 100 kPa)	Derived based on current e, λ, OCR, and R^*	0.9
u	$K_0 = 0.19 + 0.233 \log I_P$ $K_0 = 0.44 + 0.0042 I_P$	0.3
λ	$C_c = (0.3608 \times e_0) - 0.0713$	0.2
κ	$\lambda/\kappa = 5$	0.02
M	$M = \frac{6 \sin \varphi'}{3 - \sin \varphi'}$	1.2
m	Using empirical values, the clay layer is taken as 2–5, the clayey silt/silty clay layer is taken as 0.2–2, and the sandy soil layer is taken as 0.02–0.2	2.5
$\gamma_{0.7}$	Using empirical values and considering the discreteness of soil properties, it is recommended to take a value of $(1.0 \sim 3.0) \times 10^{-4}$	0.0002
OCR	$OCR = 0.37\left(\frac{q_c - \sigma_{vo}}{\sigma'_{vo}}\right)^{1.01}$	5

4.3. Orthogonal Experimental Design

The constitutive model operates as a stress–strain system influenced by a multitude of parameters. The conclusions drawn from the sensitivity analyses that vary only a single parameter may represent the behavior of the constitutive system under specific conditions, potentially leading to a one-sided understanding. Consequently, this study conducted a comprehensive sensitivity analysis to account for the collective impact of various research parameters on key indicators in foundation pit engineering. These indicators include the lateral displacement of the retaining wall, the settlement of surface soil outside the pit, and the uplift of soil at the bottom of the pit [36–39].

To simplify the calculation workload, an orthogonal experiment was used to design a two-factor, six-level orthogonal experiment with a total of 36 groups. The orthogonal experimental design is shown in Table 4.

Table 4. Six levels of values for each input parameter.

Research Parameters	λ	κ
Level 1	0.02	0.002
Level 2	0.04	0.004
Level 3	0.1	0.01
Level 4	0.2	0.02
Level 5	0.4	0.04
Level 6	0.8	0.08

4.4. Sensitivity Analysis Method

In sensitivity analysis, a sensitivity coefficient μ can be calculated for different parameter changes. This coefficient is the ratio of the percentage change in output results to the percentage change in input parameters [40], defined as follows:

$$\mu = \left| \frac{\frac{f(x+\Delta x)-f(x)}{f(x)}}{\frac{\Delta x}{x}} \right| \quad (24)$$

In the formula, x is the input value of the research parameter; $F(x)$ is the corresponding calculation result; Δx is the change in the input parameter; and $F(x + \Delta x)$ is the calculated result corresponding to the input parameter $x + \Delta x$.

4.5. Analysis of Orthogonal Experiment Results

When analyzing the results of orthogonal experiments, there are usually two methods: range analysis (visual analysis) and analysis of variance. In this experiment, range analysis was used for the result analysis.

Thirty-six sets of parameters were entered, the deformation data of the foundation pit were selected when the final excavation was completed, and the calculation results were read when the deformation was stable, as shown in Table 5. Using the orthogonal assistant, the mean and range of the two parameters that affect the lateral displacement of the diaphragm wall, the settlement of the surface soil outside the pit, and the uplift of the soil at the bottom of the pit in the orthogonal experiment results at different levels were calculated. The analysis results are shown in Table 5 and plotted in Figure 11.

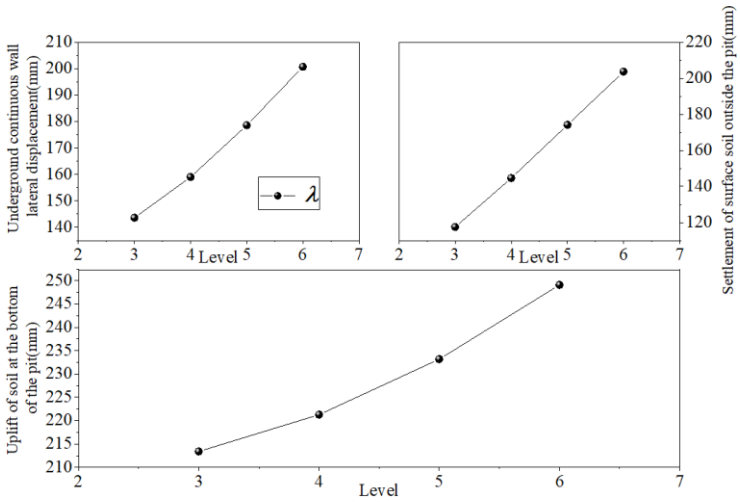

(**a**) Change analysis results for the three indicators of λ

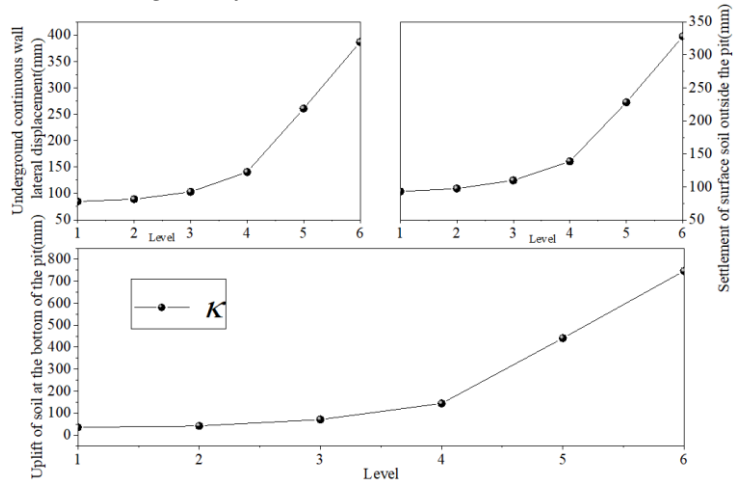

(**b**) Change analysis results for the three indicators of κ (Note: κ's single factor analysis experiment only set up six analysis gradients)

Figure 11. Orthogonal experimental research results.

Table 5. Two-factor, two-level orthogonal test design table and calculation results of analytical indicators.

Orthogonal Test	Research Parameters		Analysis Indicators		
	λ	κ	Ground-Connected Wall Lateral Displacement/mm	Surface Subsidence Outside the Pit/mm	Uplift at the Bottom of the Pit/mm
Trial 1	1	1	29.84	16.48	11.83
Trial 2	1	2	33.31	17.74	17.58
Trial 3	1	3	50.37	24.66	41.67
Trial 4	1	4	-	-	-
Trial 5	1	5	-	-	-
Trial 6	1	6	-	-	-
Trial 7	2	1	36.67	27.48	15.32
Trial 8	2	2	40.36	29.88	20.98
Trial 9	2	3	58.06	39.97	44.52
Trial 10	2	4	100.90	68.24	121.75
Trial 11	2	5	-	-	-
Trial 12	2	6	-	-	-
Trial 13	3	1	51.04	50.00	21.71
Trial 14	3	2	55.24	54.11	27.19
Trial 15	3	3	74.65	69.12	52.97
Trial 16	3	4	117.04	97.83	132.73
Trial 17	3	5	196.58	151.04	321.16
Trial 18	3	6	366.98	282.91	724.59
Trial 19	4	1	70.35	77.47	28.39
Trial 20	4	2	75.10	82.55	33.80
Trial 21	4	3	90.59	95.40	62.45
Trial 22	4	4	130.50	123.38	137.51
Trial 23	4	5	209.89	177.93	329.50
Trial 24	4	6	377.57	311.21	736.18
Trial 25	5	1	95.38	107.23	38.28
Trial 26	5	2	99.31	112.04	45.19
Trial 27	5	3	111.46	123.65	76.11
Trial 28	5	4	147.80	152.34	147.33
Trial 29	5	5	225.39	207.39	340.96
Trial 30	5	6	392.22	342.04	751.14
Trial 31	6	1	121.86	136.50	53.26
Trial 32	6	2	126.27	140.60	60.89
Trial 33	6	3	135.06	150.83	93.35
Trial 34	6	4	166.66	180.52	159.10
Trial 35	6	5	243.92	237.72	355.71
Trial 36	6	6	410.33	375.68	772.29

As λ increases, the lateral displacement of the connecting wall, the surface settlement outside the pit, and the soil uplift at the bottom of the pit increase. By increasing by the same $\Delta\lambda$, the increase in the surface settlement outside the pit is the highest, followed by the increase in the lateral displacement of the connecting wall, and the increase in the uplift at the bottom of the pit is the lowest.

An increase in kappa leads to a lateral displacement of the connecting wall, surface settlement outside the pit, and an increase in the uplift value of the soil at the bottom of the pit. By increasing by the same $\Delta\kappa$, the increase in the soil uplift at the bottom of the pit is the highest, followed by the increase in the lateral displacement of the retaining wall, and the increase in the surface settlement outside the pit is the smallest.

4.6. Parameter Sensitivity Evaluation

Due to the selection of six levels of values for λ and κ, corresponding calculation indicators can be obtained. Each parameter can be used to calculate three sensitivity coefficients, and the average value is taken as the sensitivity of each parameter. The calculation results are shown in Tables 6 and 7.

Table 6. Analysis results for range of deformation indicators for excavation.

(a) Analysis of Lateral Displacement Range of Underground Continuous Wall							
Orthogonal Test	**Ground-Connected Wall Lateral Displacement/mm**						
	Average 1	**Average 2**	**Average 3**	**Average 4**	**Average 5**	**Average 6**	**Range**
λ	-	-	143.59	159	178.59	200.68	57.09
κ	84.66	88.98	102.94	140.5	260.55	386.78	302.12
(b) Analysis of Extreme Settlement Range of Surface Soil Outside the Pit							
Orthogonal Test	**Settlement of Surface Soil Outside the Pit/mm**						
	Average 1	**Average 2**	**Average 3**	**Average 4**	**Average 5**	**Average 6**	**Range**
λ	-	-	117.50	144.66	174.12	203.64	86.14
κ	92.8	97.33	109.75	138.52	228.01	327.96	235.16
(c) Analysis of the Range of Soil Uplift at the Bottom of the Pit							
Orthogonal Test	**Uplift at the Bottom of the Pit/mm**						
	Average 1	**Average 2**	**Average 3**	**Average 4**	**Average 5**	**Average 6**	**Range**
λ	-	-	213.39	221.31	233.17	249.1	35.71
κ	35.41	41.77	71.22	144.17	440.98	746.05	710.64

Table 7. Parameter sensitivity evaluation.

Research Parameters	**Ground-Connected Wall Lateral Displacement**	**Settlement of Surface Soil Outside the Pit**	**Uplift at the Bottom of the Pit**
λ	0.057	0.105	0.024
κ	0.092	0.065	0.515

According to the sensitivity calculation results, the parameter that affects the lateral displacement of the underground continuous wall most is κ, the parameter that affects the settlement of the surface soil outside the pit most is λ, and the parameter that affects the uplift of the soil at the bottom of the pit most is κ.

5. Conclusions

The Shanghai model's parameter selection method, derived from geological survey reports, has been validated across various actual foundation pit projects. However, the current parameter selection scheme does not adequately align with actual measurements for each individual foundation pit project. This study leverages orthogonal experimental analysis results of the Shanghai model parameters, using the circular vertical shaft foundation pit of the Miaopu deep tunnel as a case study. The findings aim to offer guidance for adjusting the parameter fitting measurements of the Shanghai model to better suit actual engineering applications.

1. The suitability of the Shanghai model for simulating ultra-deep circular foundation pits in soft soil regions has been established through an analysis of the Miaopu vertical shaft foundation pit within the deep drainage and storage pipeline system project in the Suzhou River section of Shanghai. Concurrently, orthogonal experiments were

conducted to investigate the impact of variations in the λ and κ parameters of the Shanghai model on key aspects of foundation pit behavior, including the lateral displacement of the retaining wall, surface settlement outside the pit, and bottom uplift after achieving deformation stability. These experiments also assessed the sensitivity of each parameter. The principal findings are as follows:

2. Taking the Miaopu vertical shaft foundation pit in the deep drainage and storage pipeline system project of the Suzhou River section in Shanghai as an example, the excavation process of the Shanghai model foundation pit was adopted, and the calculated results and rules were consistent with the surface-measured data, reflecting the strong applicability of the Shanghai model for ultra-deep circular foundation pit engineering in soft soil areas.
3. Based on the Shanghai model mechanism, λ and κ are the key parameters for describing soil deformation in this constitutive model. Based on the orthogonal experimental data for ideal foundation pit engineering, it was shown that the lateral displacement of underground continuous walls, the surface soil settlement outside the pit, and the soil uplift at the bottom of the pit increase with the increase in the λ and κ parameters, showing obvious monotonicity.
4. In terms of sensitivity, the parameter with the highest sensitivity to the lateral displacement of the underground continuous walls is κ; the parameter with the highest sensitivity to surface subsidence outside the pit is λ; and the parameter with the highest sensitivity to bottom uplift is κ.
5. By adopting a comprehensive analysis of the full factor and multi-level values of research parameters, the influence of the parameters on the calculation results was studied and the sensitivity was evaluated, which helped strengthen our understanding of the influence of various parameters of the Shanghai model on the results in soft soil deep foundation pit engineering and identify and determine the key influencing parameters.
6. This article employed a fluid–structure interaction numerical method for deep foundation pit engineering that does not account for consolidation effects. While this approach effectively matches the observed deformations of the foundation pit, it falls short in accurately replicating the stress and deformation patterns throughout the excavation process. To enhance the accuracy and comprehensiveness of this analysis, future research should delve into numerical simulations that incorporate both fluid–structure interaction and consolidation effects.

Author Contributions: A.M.: conceptualization, methodology, field investigation, data curation, writing—original draft; W.W.: writing—review and editing; W.Z.: writing—review and editing, supervision; Z.X.: writing—review and editing, field investigation; G.Y.: conceptualization, writing—review and editing, supervision, funding acquisition. All authors have read and agreed to the published version of the manuscript.

Funding: This work received support from the Shanghai Science and Technology Commission [Grant No. 24X010502946], for which we express our deep gratitude.

Data Availability Statement: The original contributions presented in this study are included in the article. Further inquiries can be directed to the corresponding author.

Conflicts of Interest: Author Zhonghua Xu was employed by East China Architectural Design and Research Institute Co., Ltd. The remaining authors declare that the research was conducted in the absence of any commercial or financial relationships that could be construed as a potential conflict of interest.

List of Symbols

Symbol	Physical Meaning	Symbol	Physical Meaning
a	controls the rate of structural collapse	$q^{\max}$	the maximum deviatoric stress during soil-loading processes
b_r	controls the rate of anisotropy development	S_{ij}	deviatoric stress tensor
b_{r2}	controls the rate of anisotropy development before liquefaction	$1/R, 1/R_0$	the degree and initial degree of OCR
C_p	hardening parameter for plastic volumetric strain	$R^*, R^*{}_0$	the degree and initial degree of the structure
D_r	relative density	β_{ij}	anisotropic stress tensor
e	void ratio at current stress state	δ_{ij}	Kronecker delta
e_0	initial void ratio	ε_a	axial strain
$\widetilde{e}$	void ratio along the *N.C.L*	ε_{kl}	strain tensor
E_{ijkl}	elastic stiffness tensor	ε^e_{kl}	elastic strain tensor
f	yield surface	$\varepsilon^p_{ij}, \varepsilon^p_v, \varepsilon^p_d$	plastic strain tensor, plastic volumetric strain, and plastic shear strain
h	represents the influence of anisotropic stress history	ζ, ζ_0	the magnitude and initial magnitude of β_{ij}
k	controls resistance to liquefaction	η_{ij}	stress ratio tensor
m	controls the rate of OCR development	$\hat{\eta}_{ij}$	the difference between η_{ij} and β_{ij}
M	gradient of the *C.S.L*	η^*	the magnitude of $\hat{\eta}_{ij}$
N	reference void ratio	$\eta^{*\min}/\eta^{*\max}$	the minimum or maximum value of η^*
p_0	initial mean effective stress	κ	swelling index
p_m	mean effective stress	λ	compression index
p_{ref}	reference stress	Λ	positive variable
p, q	current stress state on the subloading yield surface	ν	Poisson's ratio
$\widetilde{p}, \widetilde{q}$	stress states projected onto the normal yield surface	σ_{ij}	effective stress tensor
$\overline{p}, \overline{q}$	stress states projected onto the superlaoding yield surface	σ_m	mean effective stress
q_0	initial deviator stress	σ_{ref}	reference stress
OCR	the overconsolidation ratio of soil	m^*	the development rate of m

References

1. Xu, Z.H.; Wang, W.D. Selection of soil constitutive model in numerical analysis of foundation pit under sensitive environment. *Rock Soil Mech.* **2010**, *31*, 258–264.
2. Tomassi, A.; Milli, S.; Tentori, D. Synthetic seismic forward modeling of a high-frequency depositional sequence: The example of the Tiber depositional sequence (Central Italy). *Mar. Pet. Geol.* **2024**, *160*, 106624. [CrossRef]
3. Zhang, F.; Ye, B.; Ye, G.L. Unified description of sand behavior. *Front. Archit. Civ. Eng.* **2011**, *5*, 121–150. [CrossRef]
4. Taiebat, M.; Dafalias, Y.F. SANISAND: Simple anisotropic sand plasticity model. *Int. J. Numer. Anal. Methods Geomech.* **2008**, *32*, 915–948. [CrossRef]
5. Yin, Z.Y.; Chang, C.S.; Karstunen, M.; Hicher, P.Y. An anisotropic elastic–viscoplastic model for soft clays. *Int. J. Solids Struct.* **2010**, *47*, 665–677. [CrossRef]
6. Zhou, A.N.; Sheng, D.C. An advanced hydro-mechanical constitutive model for unsaturated soils with different initial densities. *Comput. Geotech.* **2015**, *63*, 46–66. [CrossRef]
7. Thompson, M.J.; VandenBerge, D.R. Shear strength of remolded and compacted beaumont clay. In Proceedings of the Conference Geotechnical Frontiers 2017: Geotechnical Materials, Modeling, and Testing, Orlando, FL, USA, 12–15 March 2017; pp. 82–91. [CrossRef]

8. Lau, W.H.W. The Behaviour of Clay in Simple Shear and Triaxial Tests. Doctoral Dissertation, City University London, London, UK, 1988.
9. Hattab, M.; Hicher, P.Y. Dilating behaviour of overconsolidated clay. *Soils Found.* **2004**, *44*, 27–40. [CrossRef]
10. Zhang, F. *Computational Soil Mechanics*; China Communications Press: Beijing, China, 2007.
11. Sheng, J.R.; Ye, G.L.; Wang, J.H. Soil-water coupled numerical simulation on underground cavern excavation in soft rock ground. *J. Zhejiang University Eng. Sci.* **2012**, *46*, 785–790.
12. Yang, T.-S.; Ye, G.-L.; Gu, L.-L. Small-strain triaxial tests and constitutive modeling of Shanghai soft clays. *Chin. J. Geotech. Eng.* **2018**, *40*, 1930–1935.
13. Zhang, H.; Yang, S.-F.; Wang, L.; Lin, T.-X. Experimental researches on in-situ loading and unloading deformation characteristics of soft soil based on pressuremeter tests in Shanghai area. *Chin. J. Geotech. Eng.* **2022**, *44*, 769–777.
14. Liang, F.-Y.; Jia, Y.-J.; Ding, Y.-J.; Huang, M.-S. Experimental study on parameters of HSS model for soft soils in Shanghai. *Chin. J. Geotech. Eng.* **2017**, *39*, 269–278.
15. Hu, F.; Shi, G.; Shi, Y. Constitutive model for full-range elasto-plastic behavior of structural steels with yield plateau: Calibration and validation. *Eng. Struct.* **2016**, *118*, 210–227. [CrossRef]
16. Ye, G.L.; Ye, B. Investigation of the overconsolidation and structural behavior of Shanghai clays by element testing and constitutive modeling. *Undergr. Space* **2016**, *1*, 62–77. [CrossRef]
17. Yin, J. Application of hardening soil model with small strain stiffness in deep foundation pits in Shanghai. *Chin. J. Geotech. Eng.* **2010**, *32*, 166–172.
18. Xu, Z.; Li, J.; Wang, Q. Analysis method of ultra-deep circular excavation and its application. *Constr. Technol.* **2022**, *51*, 13–20.
19. Wang, W.; Xu, Z.; Zong, L. Optimal design and practice of a 56 m ultra-deep circular excavation in soft soils. *Build. Struct.* **2022**, *52*, 1–10.
20. Asaoka, A.; Nakano, M.; Noda, T. Soil-water coupled behaviour of saturated clay near/at critical state. *Soils Found.* **1994**, *34*, 91–105. [CrossRef]
21. Zhang, D.; Zhou, Y.; Phoon, K.K.; Huang, H. Multivariate probability distribution of Shanghai clay properties. *Eng. Geol.* **2020**, *273*, 105675. [CrossRef]
22. Tanoli, A.Y.; Ye, G.L. Numerical modeling of excavation in Shanghai soft clays using the new small strain Shanghai constitutive model. In *New Approaches of Geotechnical Engineering: Soil Characterization, Sustainable Materials and Numerical Simulation: Proceedings of the 6th GeoChina International Conference on Civil & Transportation Infrastructures: From Engineering to Smart & Green Life Cycle Solutions—Nanchang, China*; Springer International Publishing: Berlin/Heidelberg, Germany, 2021; Volume 6, pp. 80–94.
23. Xie, W.B.; Zhang, Q.; Ye, G.L. Influence of repeated surface surcharge loading on tunnel displacement considering the structural characteristics of soft clay. In *IOP Conference Series: Earth and Environmental Science*; IOP Publishing: Bristol, UK, 2024; Volume 1330, p. 012019.
24. Asaoka, A.; Noda, T.; Yamada, E.; Kaneda, K.; Nakano, M. An elasto-plastic description of two distinct volume change mechanisms of soils. *Soils Found.* **2002**, *42*, 47–57. [CrossRef]
25. Burland, J.B. Small is beautiful-the stiffness of soils at small strain. *Can. Geotech. J.* **1989**, *26*, 499–516. [CrossRef]
26. Santos, J.A.; Correia, A.G. Reference threshold shear strain of soil. Its application to obtain an unique strain-dependent shear modulus curve for soil. In Proceedings of the 15th International Conference on Soil Mechanics and Geotechnical Engineering, Istanbul, Turkey, 27–31 August 2001; pp. 267–270.
27. Yu, Y.; Ye, G.; Xiong, Y. Elastoplastic constitutive modelling for mechanical behavior of Shanghai 4th layer clay. *Rock Soil Mech.* **2016**, *37*, 2541–2546.
28. Di Marzo, M.; Tomassi, A.; Placidi, L. A Methodology for Structural Damage Detection Adding Masses. *Res. Nondestruct. Eval.* **2024**, *35*, 172–196. [CrossRef]
29. Dong, Y.P.; Burd, H.J.; Houlsby, G.T. Finite-element analysis of a deep excavation case history. *Géotechnique* **2016**, *66*, 1–15. [CrossRef]
30. Hsieh, P.G.; Ou, C.Y. Shape of ground surface settlement profiles caused by excavation. *Can. Geotech. J.* **1998**, *35*, 1004–1017. [CrossRef]
31. Zhang, W.S.; Yuan, Y.; Long, M.; Yao, R.H.; Jia, L.; Liu, M. Prediction of surface settlement around subway foundation pits based on spatiotemporal characteristics and deep learning models. *Comput. Geotech.* **2024**, *168*, 106149. [CrossRef]
32. Ye, S.; Zhao, Z.; Wang, D. Deformation analysis and safety assessment of existing metro tunnels affected by excavation of a foundation pit. *Undergr. Space* **2021**, *6*, 421–431. [CrossRef]
33. Xu, Q.; Xie, J.; Lu, L.; Wang, Y.; Wu, C.; Meng, Q. Numerical and theoretical analysis on soil arching effect of prefabricated piles as deep foundation pit supports. *Undergr. Space* **2024**, *16*, 314–330. [CrossRef]
34. Capehart, T.W.; Cheng, Y.T. Determining constitutive models from conical indentation: Sensitivity analysis. *J. Mater. Res.* **2003**, *18*, 827–832. [CrossRef]

35. Zhao, C.; Lavasan, A.A.; Barciaga, T.; Zarev, V.; Datcheva, M.; Schanz, T. Model validation and calibration via back analysis for mechanized tunnel simulations–The Western Scheldt tunnel case. *Comput. Geotech.* **2015**, *69*, 601–614. [CrossRef]
36. Zhang, J.X.; Zhao, G.; Zhang, L.; Jiang, H. Application of HSS model in shield simulation and parameter sensitivity research. *Chin. J. Undergr. Space Eng.* **2020**, *16*, 618–625.
37. Houhou, M.N.; Emeriault, F.; Belounar, A. Three-dimensional numerical back-analysis of a monitored deep excavation retained by strutted diaphragm walls. *Tunn. Undergr. Space Technol.* **2019**, *83*, 153–164. [CrossRef]
38. Zeng, C.F.; Zheng, G.; Zhou, X.F.; Xue, X.L.; Zhou, H.Z. Behaviours of wall and soil during pre-excavation dewatering under different foundation pit widths. *Comput. Geotech.* **2019**, *115*, 103169. [CrossRef]
39. Tan, Y.; Wang, D. Characteristics of a large-scale deep foundation pit excavated by the central-island technique in Shanghai soft clay. I: Bottom-up construction of the central cylindrical shaft. *J. Geotech. Geoenviron. Eng.* **2013**, *139*, 1875–1893.
40. Shi, Y.; Ruan, J.; Wu, C. Xiamen area typical stratum of HS-small model for small strain parameters sensitivity analysis. *Sci. Technol. Eng.* **2017**, *17*, 105–110.